

NEUTRON INDUCED EFFECTS IN A MONOLITHIC ACTIVE PIXEL SENSOR: THE MIMOSA8 CHIP

CEA/DAPNIA summary report

N. T. Fourches, 02/06/06

Co workers:

M. Besançon, Y. Degerli, Y. Li, P. Lutz, F. Orsini

PERMANENT EFFECTS AT MODERATE CLOCKING FREQUENCY (1 MHz):

1-Introduction

In this study the chips studied were MIMOSA8 chips developed at CEA/Saclay and IRES/IPHC/Strasbourg and manufactured by TSMC through MOSIS. They are based on the pixel architecture which comprises in-situ amplification and correlated double-sampling. Auto-zero discrimination is implemented at the bottom of some columns for the digital outputs which were not used in this study. For the analog outputs the useful signal is the difference between a reference signal (calibration) and the readout signal (read) and is computed by software. The DAQ card was developed at IRES/LEPSI (Strasbourg). Seven chips were irradiated at four different integrated fluxes. A few un-irradiated reference chips were measured.

2-Structure of the pixel diode and bulk effects

In epitaxial processes, such as the one used for the MIMOSA8 prototype (TSMC 0.25 μm) the degradation due to neutron irradiation is mostly due atomic displacements in the thin epitaxial layer (a few μm). A number of point defects and defect clusters are created; this reduces the lifetime of the minority carriers (in these case electrons) and induces deep traps that affect the transport properties in the silicon.

There are clearly two kinds of effects.

First a continuous or so effect is the increase of the generation-recombination current in the depleted region of the n+p junction of the sensing element. This current is integrated on the sensing node and can be probed in this way. This current is directly related to the electron lifetime and normally increases when the neutron exposure is enhanced.

Second carrier capture affects the free drift length of the electrons or their diffusion length. In the case of the MAPS (Monolithic Active Pixel Sensors) electron transport mainly occurs by diffusion as the applied electric field in the sensor is extremely low. If σ_n is the capture cross section for electrons, the free drift length is deduced from: $N_t \nu \sigma_n$ where N_t is the deep trap concentration. This is valid for one type of trap only. The free drift length is then: $L = 1 / (N_t \sigma_n)$. L is reduced when the trap concentration increases, along with neutron integrated flux. A similar conclusion can be drawn with the diffusion length which is given by: $L = (D_n \tau_n)^{0.5}$.

The lifetime is reduced when the trap concentration increases and this induces a reduction of the diffusion length. The lifetime is related to the trap concentration (for a single kind of trap) by: $(vN_t\sigma_n)^{-1}$. In this work the devices have been measured at a 1 MHz clocking frequency up to $1.13 \cdot 10^{13}$ neutrons/cm². The neutron flux has a spectrum which extends up to 20 MeV [1], as indicated in Figure 1.

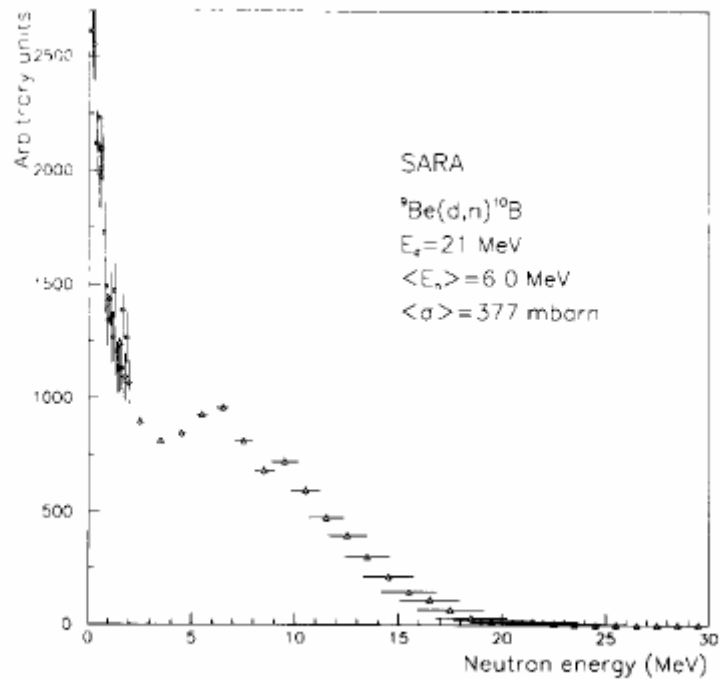


Fig. 4. Neutron energy spectrum measured at 0° with a threshold of 100 keV.

Figure 1: Neutron flux as a function of energy for the source used (J. Collot et al., this Figure (Fig 4) was reprinted from J. Collot et al., Nucl. Inst. and Meth. In Physics Research, A 350, 525-529 (1994))

3- Effects on the pedestals:

For the MIMOSA8 chip the analog outputs are processed in order to subtract the voltage levels present before and after reset. This enables the extraction of the useful signal and a reduction of the pedestals. The residual pedestals (offset) are related to the characteristics of the sensing elements and the material. Figure 2 (a) (b) shows the distribution of pedestals on four columns of the array for a sample irradiated at the maximum integrated flux and at the minimum integrated flux. Figure 3 and Figure 4 show the variation of the pedestals with integrated flux for the central columns and the lateral columns.

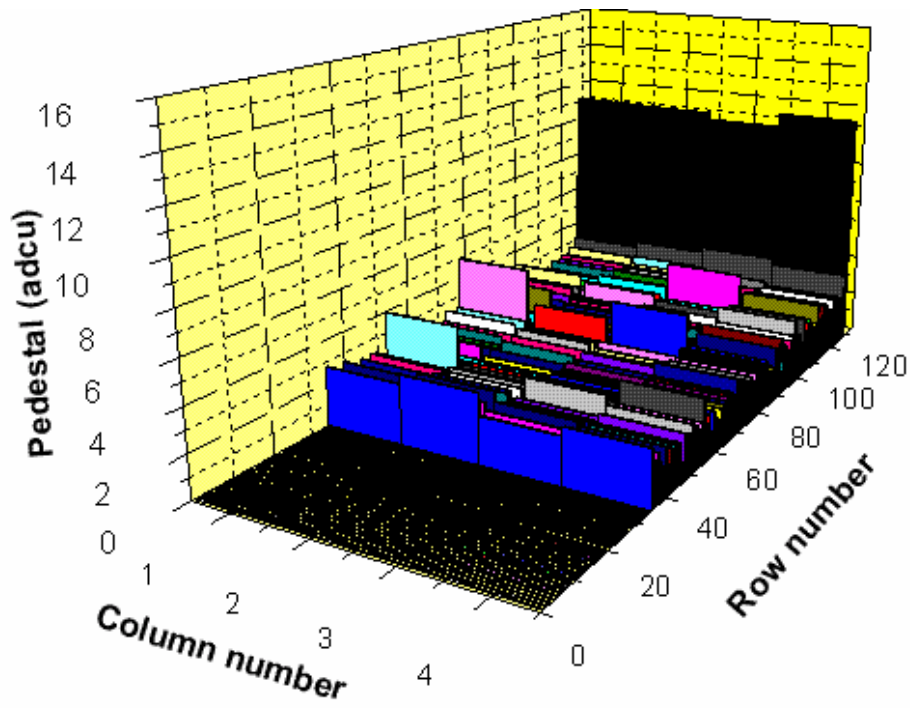


Figure 2 (a): distribution of pedestals on a subarray of four columns (central) for a chip irradiated at 1.44×10^{11} neutrons/cm².

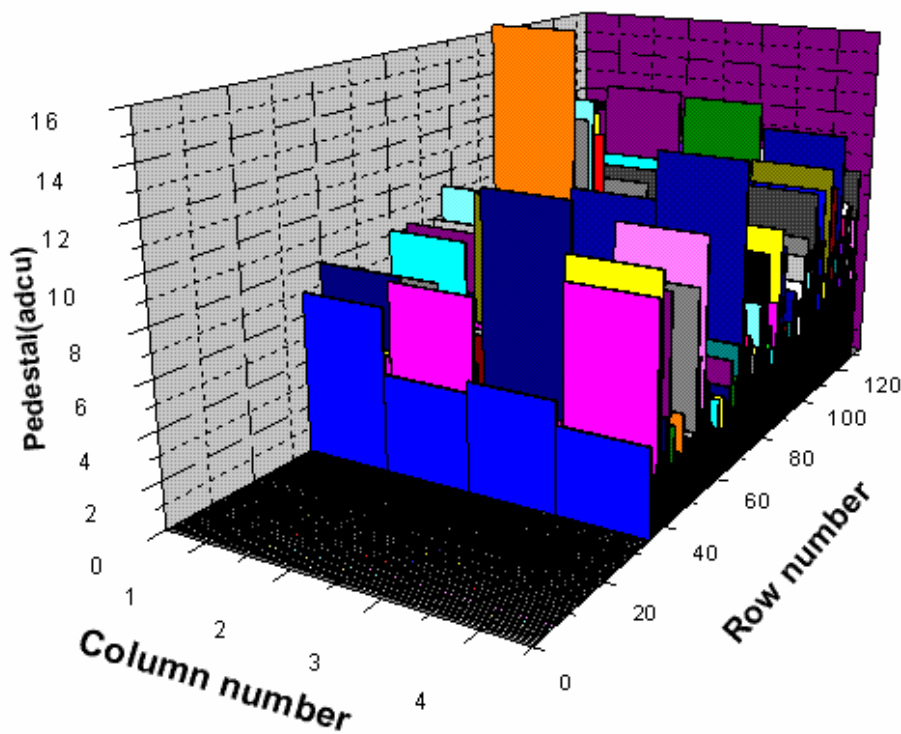


Figure 2 (b): distribution of pedestals on a subarray of four columns (central) for a chip irradiated at 1.13×10^{13} neutrons/cm².

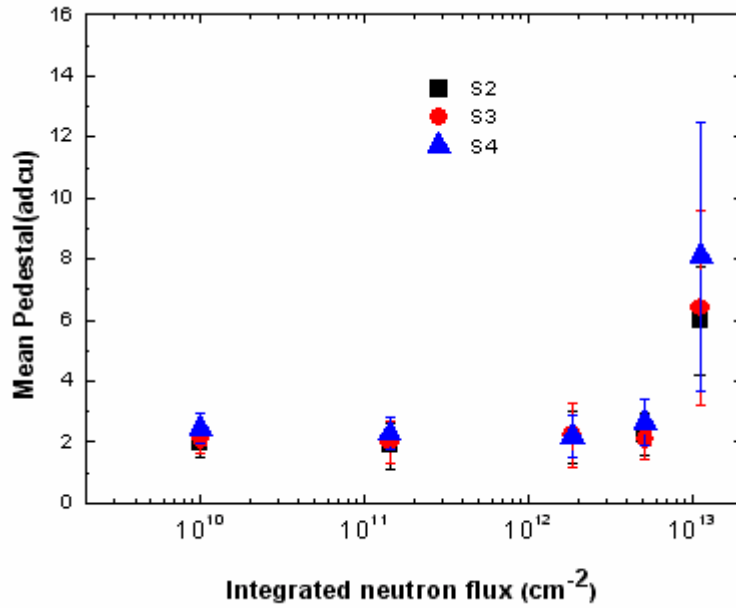


Figure 3: (mean) pedestals versus neutron integrated flux for the central columns. All the four columns were taken; the first point (on the left side of the plot) corresponds to a non irradiated sample. The error bars correspond to the sigma on the pedestals.

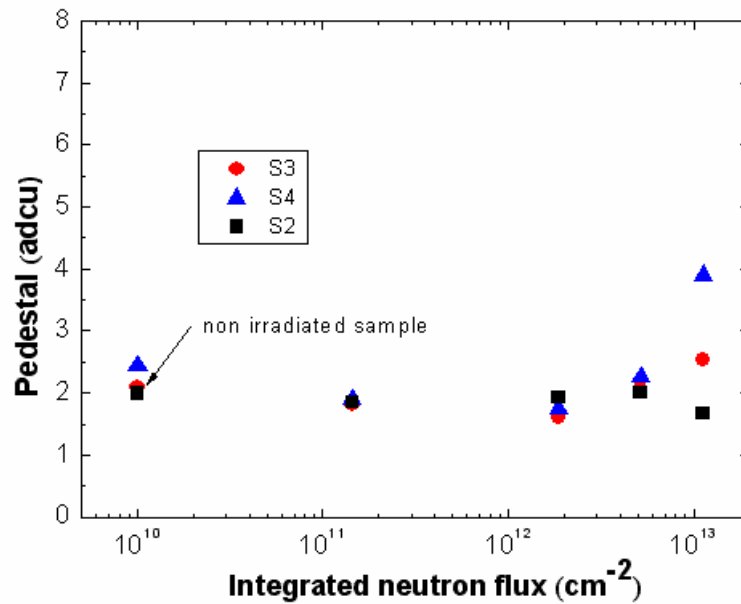


Figure 4: pedestals versus neutron integrated flux for the lateral columns. All the four columns were taken; the first point (left) corresponds to a non irradiated sample. No errors bars are included here.

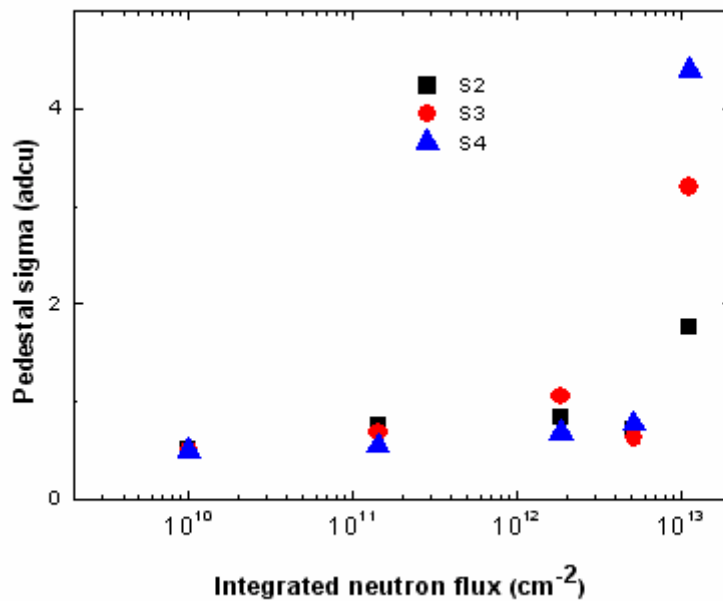


Figure 5: pedestal sigma (fixed pattern noise) versus integrated neutron flux for the 3 sub-arrays studied. All the four central columns were taken in the computation.

Two conclusions can be drawn; first the pedestals mean value increase with total integrated neutron flux and second the dispersion between pedestals increases with the total integrated flux. This behaviour does not depend on the column as it can be seen on Figure 2. The two plots show that for the S4 sub-array the Fixed Pattern Noise (Pedestal Sigma) varies of a factor 8 or more starting from an un-irradiated sample to the most irradiated one. The Pedestals alone only varies in a factor 4. This proves that the dispersion increases with integrated flux in this range. The dispersion between neighbouring pixels (as it can be observed in Fig 2) may find its origin in the non-homogeneous distribution of neutron induced defects in the sensitive silicon epitaxial layer. At higher integrated fluxes it should be clear that because of the size of the radiation induced defects the defect concentration should be more homogeneous (see §4).

It is clear that a sharp increase occurs for the highest integrated flux as it will be explained in the following paragraph.

Moreover the dispersion of the pedestals (the fixed pattern noise) increases with the integrated neutron flux (Figure 5). This is directly related to the distribution of neutron induced clusters as it will be discussed next.

4-Temporal noise:

The temporal noise of the three sub-arrays is weakly dependent on the total integrated flux. There is no perceptible noise increase. Flicker noise due the increased concentration of radiation induced traps should be a major source of bulk detector noise. At this stage of the study it is difficult to assess the respective contributions of these noise sources (Figure 6). Most of the noise is due to the electronic noise.

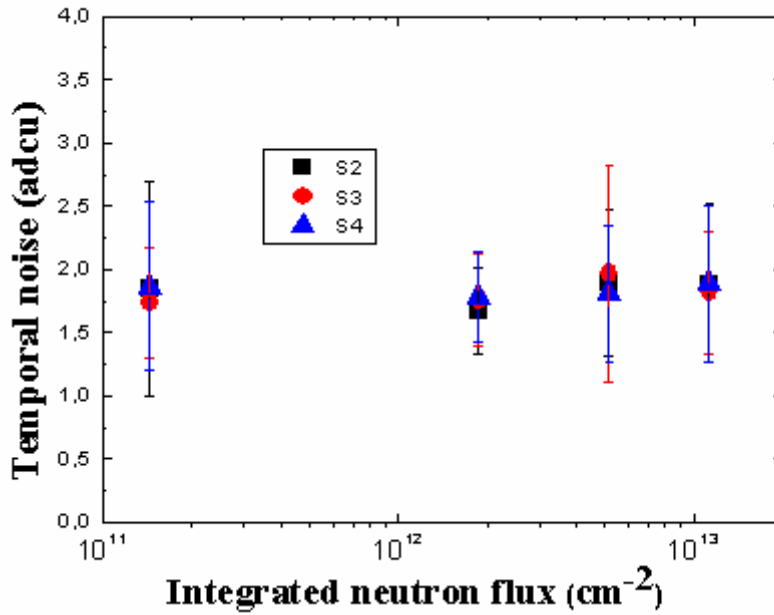


Figure 6: Temporal noise versus integrated neutron flux in adc units for the three sub arrays.

5-Interpretation:

Previous work shows that irradiation by massive particles in semiconductors produce defects that trend to form clusters of significant spatial extension up to 1 μm [2][3][4].

The collision cross section for 1 MeV neutrons on silicon is approximately $3 \cdot 10^{-24} \text{ cm}^2$ [5]. Simple calculations show that for an integrated flux of 10^{13} neutrons/cm² the total number of atomic collisions per squared centimetre is of the order of 10^8 collisions /cm², assuming a 10 μm epitaxial layer thickness. For a 25 μm large pixel the number of primary collisions in the epi-layer is roughly 5. For MeV energetic neutrons each primary collision induces a cascade of approximately 500 secondary displacements. The threshold energy for atomic displacements in silicon is 20 eV and the energy of the Primary Knock on Atom (PKA) is roughly 36 keV on average, leading to around 500 atomic displacements (for the principle of the calculation see [6] and [7]). As a result the concentration of primary point defects in the active region of the pixel lies near 2500. This relatively low value may explain the important dispersion of the pedestal values after irradiation. For integrated fluxes 100 times lower (10^{11} neutrons/cm²), the number of defects below each pixel has an average lower than 5. This indicates that the effect of neutron irradiation at this integrated flux is very low as it can be seen in Figure 2(a). Moreover as the number of primary collisions per pixel is close to unity even at high integrated fluxes the spatial extension of the defects (1 μm in average) results in defect clusters non-homogeneously distributed in the pixel inducing a possible dispersion of leakage currents in the sensor. This is the basic explanation of the dispersion of the pedestals through the array. In addition the number of primary collisions in a cluster of 9 pixels is 45 for 10^{13} neutrons/cm². This may indicate that for integrated fluxes $2 \cdot 10^{11}$ neutrons/cm² the effects of irradiation should be very much reduced. The dispersion of these pedestals should saturate if the total defect concentration is further increased by irradiation. This should be confirmed experimentally.

6- Charge collection efficiency:

The charge collection efficiency (CCE) is here defined as the ratio of the position (MPV of signal amplitude) of the peak corresponding to 9 pixels clusters to the calibration peak (total collection of the charge). The clusters are here calculated in a 4 columns to 32 rows sub-array. The charge collection efficiency is directly related to the electron transport properties in the silicon. The deep traps reduce the average electron migration length and lower the average signal amplitude through various signal build up mechanisms. Simulations could help to quantitatively evaluate the effects of neutron-induced deep traps on the signal formation.

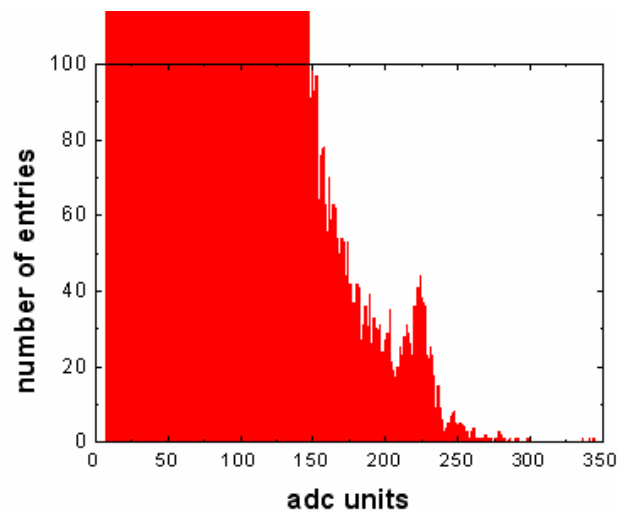


Figure 7(a): calibration (total absorption) peak for the lowest integrated flux (1 adcu=0.5 mV):

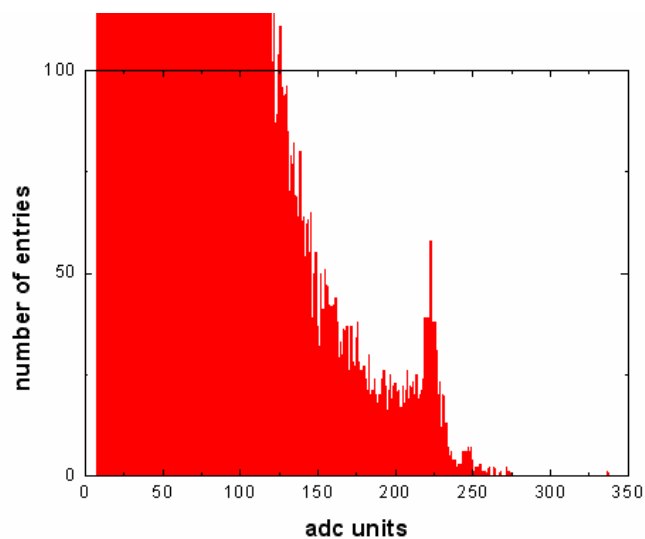


Figure 7(b): calibration (total absorption) peak for the highest integrated flux (1 adcu=0.5 mV):

Experimentally the calibration peak shape does not change greatly with integrated flux (Figure 7(a) (b)). The cluster peak shifts towards lower values leading to reduced charge collection (Figure 8 for the highest irradiation). The signal is measured by and ADC inside the DAQ board at the output of the measurement board (proximity PCB).

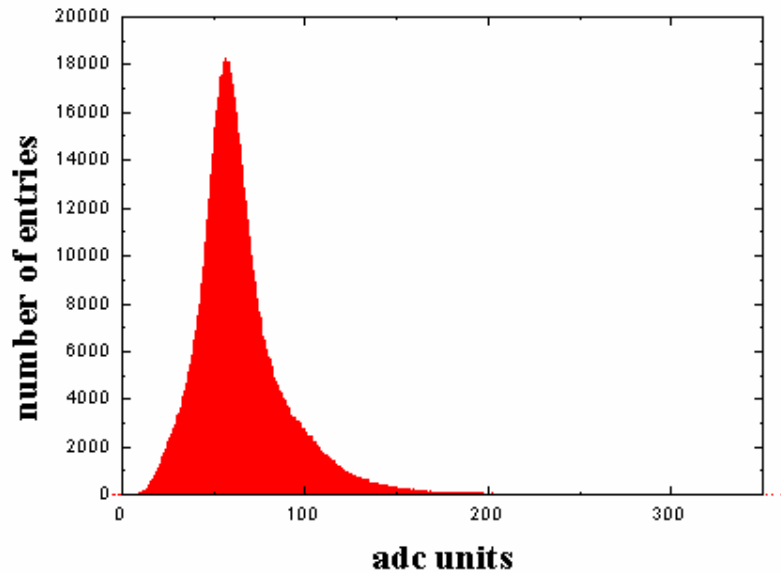


Figure 8: cluster peak (9 pixels) for the highest integrated flux (1 adcu=0.5 mV).

The charge collection efficiency plotted versus integrated neutron flux is given in Figure 9.

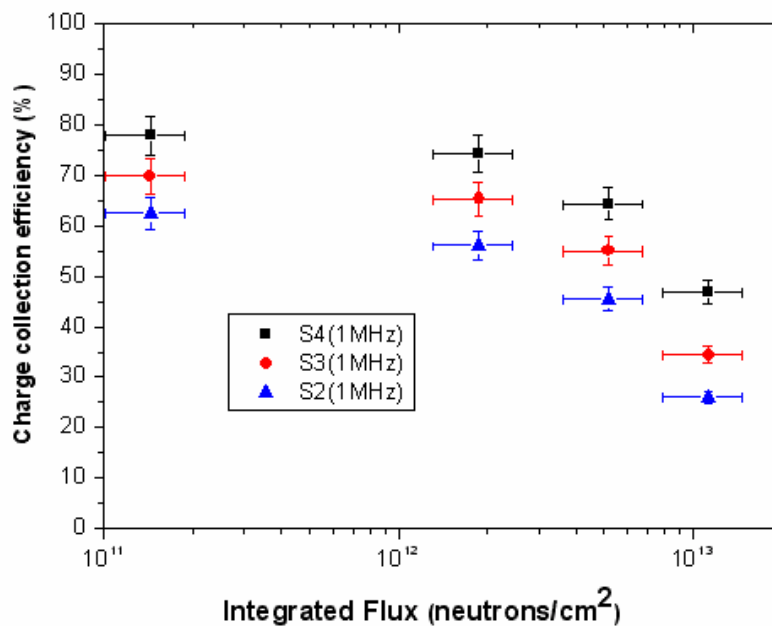


Figure 9 (a): charge collection efficiency versus integrated neutron flux for the three sub-arrays studied (log scales).

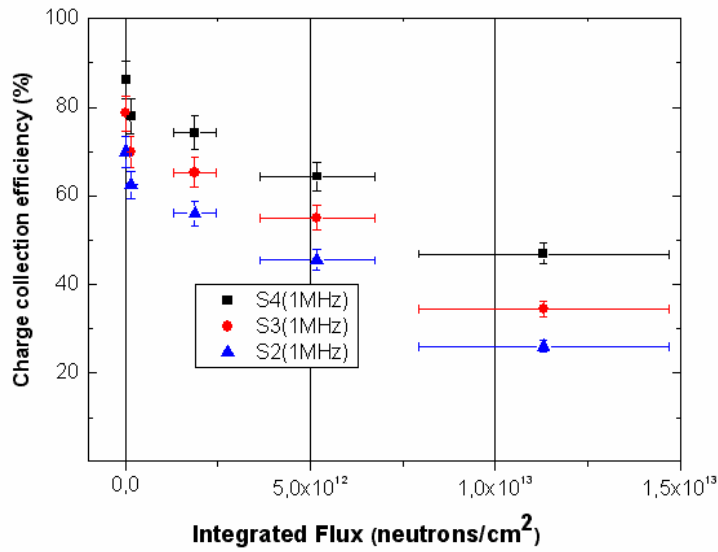
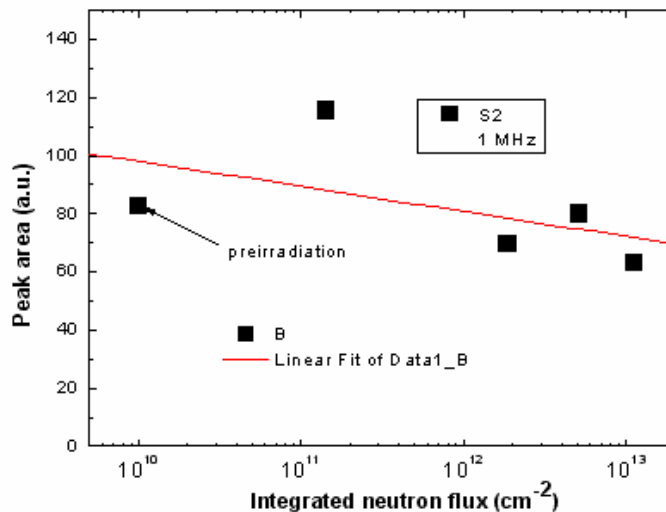
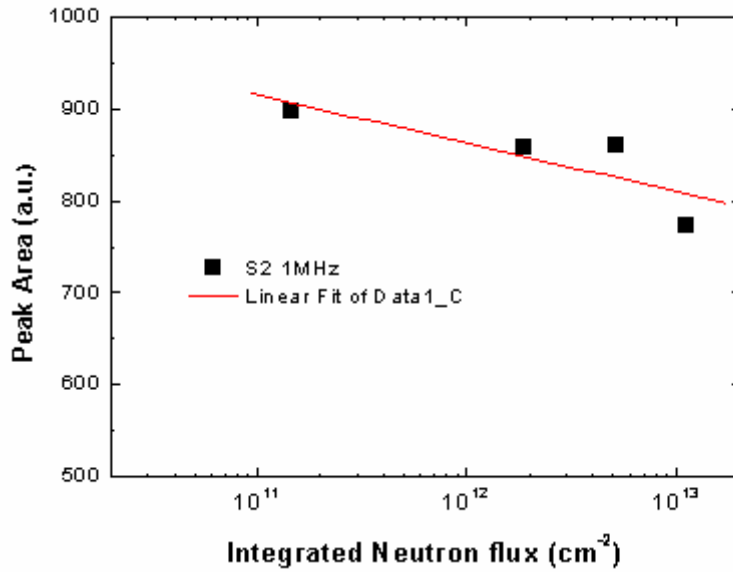


Figure 9 (b): charge collection efficiency versus integrated neutron flux for the three sub-arrays studied (linear scales). The point at the origin is that of an un-irradiated chip.

It is clear that the CCE decreases sharply for integrated fluxes above 10^{12} neutrons/cm². In this case as the pixel clusters have an area 9 times the area of one single pixel, the sensitivity to neutron irradiation is increased. Thus CCE is more affected by irradiation than the pedestals. In addition Figure 10 shows the area of the calibration peak versus the integrated neutron flux for the S2 sub-array. A trend appears which shows that the number of calibration events slightly decreases when the integrated flux increases. This is easily understandable: the calibration peak is made up by rare events (hits) that result in an almost total collection of the generated carriers (electrons). As the concentration of radiation induced defects increases the number of carriers collected with no capture decreases sharply. This is made understandable by the simple calculations presented in the first paragraph.



(a) area of the pedestal component of the calibration peak



(b) area of the gaussian component of the calibration peak minus pedestal

Figure 10 (a) (b): area of the calibration peak versus integrated flux (S2 sub-array) with a linear fit. The peak area is deduced from a fit with a normal law with a residual pedestal.

7- Leakage current: interpretation

For the clocking frequency of 1 MHz the time interval between two readouts is $128 \times 1\mu\text{s} \times 16 = 2.048 \text{ ms}$ (rigorously speaking $2.048 \text{ ms} - 16 \mu\text{s}$). When no events occur this is the time interval between which the leakage current is effective in changing the pedestals. For the highest integrated neutron flux and the largest diode (S4) the pedestal value is around 8 adcu, corresponding to 4 mV. This means that the slew rate is given by: $dV/dt = 4 \text{ mV}/2.032\text{ms} = 1.97 \text{ V/s}$. For the S4 sub-array the conversion factor is $55 \mu\text{V/e-}$, equivalent to $3.42 \cdot 10^{14} \text{ Volt/Coulomb}$. The capacitance at the sensing node is then $2.92 \cdot 10^{-15} \text{ F}$ or 2.92 fF. The leakage current is then given by: $i=C(dV/dt) = 1.97 \times 2.92 \cdot 10^{-15} = 5.75 \cdot 10^{-15} \text{ A} = 5.75 \text{ fA}$. This value is relatively weak and proves that the recombination-generation current remains low.

$J = qW \langle N_t \rangle \sigma_p \sigma_n v_{th} n_i / (\sigma_n + \sigma_p)$ is the current density in the diode due to recombination processes.

With $W \sim 1\mu\text{m}$, order of magnitude of the depletion region below the n+ région;

$$\sigma_n = \sigma_p = 10^{-15} \text{ cm}^2, v_{th} \sim 10^7 \text{ cm.s}^{-1}, n_i \sim 1.45 \cdot 10^{10} \text{ cm}^{-3}.$$

$J \sim \langle N_t \rangle 1.17 \cdot 10^{-21} \text{ A/cm}^2$. The concentration of traps can be computed with a current density of: $J \sim 0.0998 \cdot 10^{-6} \text{ A/cm}^2$ assuming squared diode ($2.4 \mu\text{m} \times 2.4 \mu\text{m}$). The trap concentration is then: $\langle N_t \rangle \sim 8.53 \cdot 10^{13} \text{ cm}^{-3}$. This gives an electrically active defect introduction rate of approximately: $K = \langle N_t \rangle / \Phi = 7.5 \text{ cm}^{-1}$. This value should be compared to the value of 5 cm^{-1} that can be deduced from the numerical estimations introduced in paragraph 5 or to other experimental values [8].

8- Conclusion

This study should be completed in the future by an investigation of the influence of the clocking frequency on the basic characteristics of the device. At present the results show that for integrated fluxes lower than 10^{12} neutrons/cm² the effects on the pedestals, the CCE and the temporal noise is insignificant. This readily proves that the present characteristics of the MIMOSA8 chips are sufficient to satisfy the needs of the future linear colliders, in terms of the atomic displacement effects due to neutrons.

ACKNOWLEDGEMENTS:

The neutron irradiations were performed at the CERI (CNRS) at Orléans (France). The assistance of J. Briaud and co-workers (CERI, Orléans) during irradiation and for dosimetry is gratefully acknowledged. Some of the nickel samples used for dosimetry was kindly provided by an IN2P3/Orsay technical group. I specially acknowledge the valued work of my colleagues Y. Degerli for his involvement in the design of the chip, Y. Li for the development of the software. The contribution of our colleagues in IRES/ULP for the Data Acquisition developments is also acknowledged.

REFERENCES:

- [1] J. Collot et al., Nucl. Inst. and Meth. In Physics Research, A 350, 525-529 (1994)
- [2] Rohn Truell, Phys. Rev., 116, 890-892 (1959)
- [3] N. Fourches, J. Appl. Phys. 77 (8), 3684 (1995)
- [4] M. Huhtinen, Nucl. Inst. and Meth. In Physics Research A, 491, 194-215 (2004)
- [5] G.C. Messenger, IEEE Transactions on Nuclear Science, Vol 39, No 3, 468 (1992)
- [6] N. Fourches, Doctoral Thesis, Université Louis Pasteur (1989)
- [7] P. Sigmund, Appl. Phys. Letters, Volume 14, Number 3, 114 (1969)
- [8] H.J. Stein and R. Gereth, J. Appl. Phys. Vol 39, No6, 2890-2904 (1968)